Mapping of m⁶A and Its Regulatory Targets in Prostate Cancer Reveals a METTL3-Low Induction of Therapy Resistance

Kellie A. Cotter[1], John Gallon[2], Nadine Uebersax[1], Philip Rubin[1], Kate D. Meyer[3,4], Salvatore Piscuoglio[2,5,6], Samie R. Jaffrey[7], and Mark A. Rubin[1,8,9]

ABSTRACT

Recent evidence has highlighted the role of N^6-methyladenosine (m⁶A) in the regulation of mRNA expression, stability, and translation, supporting a potential role for posttranscriptional regulation mediated by m⁶A in cancer. Here, we explore prostate cancer as an exemplar and demonstrate that low levels of N^6-adenosine-methyltransferase (*METTL3*) is associated with advanced metastatic disease. To investigate this relationship, we generated the first prostate m⁶A maps, and further examined how METTL3 regulates expression at the level of transcription, translation, and protein. Significantly, transcripts encoding extracellular matrix proteins are consistently upregulated with

METTL3 knockdown. We also examined the relationship between METTL3 and androgen signaling and discovered the upregulation of a hepatocyte nuclear factor–driven gene signature that is associated with therapy resistance in prostate cancer. Significantly, METTL3 knockdown rendered the cells resistant to androgen receptor antagonists via an androgen receptor–independent mechanism driven by the upregulation of nuclear receptor *NR5A2/LRH-1*.

Implications: These findings implicate changes in m⁶A as a mechanism for therapy resistance in metastatic prostate cancer.

Introduction

At the molecular level, prostate cancer is generally characterized by large-scale structural genomic rearrangements (1, 2) and relatively few recurrent genomic alterations (3, 4), which thus far are insufficient to explain the heterogeneity of the disease and suggest the importance of other mechanisms for gene regulation. In particular, multiomics studies in prostate cancer have demonstrated that for many oncogenes, copy-number alterations, DNA methylation, and even mRNA abundance are insufficient to explain the variation seen in protein expression (5, 6), emphasizing a sizeable role for posttranscriptional gene regulation in prostate cancer.

Analogous to epigenetic modifications of DNA, mRNA is also subject to multiple biochemical modifications, the most prevalent being N^6-methyladenosine (m⁶A; ref. 7). m⁶A is a dynamic mRNA modification and is regulated by the methyltransferase "writer" complex (METTL3, METTL14, WTAP, VIRMA, ZC3H13, and RBM15; refs. 8–12), the demethylase "eraser" (ALKBH5; ref. 13), and "reader" proteins (YTHDF1/2/3; refs. 14, 15). m⁶A is found on approximately 25% of all transcripts, and is unevenly distributed, with the majority of residues localized near the stop codon or in 3′ untranslated regions (UTR). Mechanistically, m⁶A has been shown to both destabilize mRNA transcripts (9, 15, 16) and increase translation (17), in addition to influencing splicing (14, 18) and miRNA processing (19).

Alterations in m⁶A have been associated with progression of multiple cancer types. In glioblastoma and breast cancer, increased expression of the demethylase ALKBH5 and concurrent reduced levels of m⁶A were implicated in the promotion of tumorigenesis and self-renewal of stem-like cells by stabilizing key mRNAs (e.g., the pluripotency factor *NANOG*; refs. 20–22). In contrast, in lung adenocarcinoma and myeloid leukemia, elevated expression of METTL3 promoted the translation efficiency (TE) of several important oncogenes and enhanced cell growth and invasion (23, 24). Lastly, *METTL3* has been shown to be both highly expressed in prostate cancer, and essential for proliferation in multiple prostate cancer cell lines (25–27), strongly supporting the significance of m⁶A methylation in prostate cancer.

Of particular concern clinically is metastatic, castration-resistant prostate cancer (CRPC) in which the disease develops resistance to both first-line treatment with androgen deprivation therapy, and to second-generation androgen receptor (AR) signaling inhibitors [ARSi, i.e., abiraterone or enzalutamide (ENZ); ref. 28]. There are several proposed mechanisms of resistance that lead to CRPC including alterations in AR which permit activity in low-androgen settings,

[1]Department for BioMedical Research, University of Bern, Bern, Switzerland. [2]Visceral Surgery and Precision Medicine Research Laboratory, Department of Biomedicine, University of Basel, Basel, Switzerland. [3]Department of Biochemistry, Duke University School of Medicine, Durham, North Carolina. [4]Department of Neurobiology, Duke University School of Medicine, Durham, North Carolina. [5]Institute of Medical Genetics and Pathology, University Hospital Basel, Basel, Switzerland. [6]Clarunis, Department of Visceral Surgery, University Centre for Gastrointestinal and Liver Diseases, St. Clara Hospital and University Hospital Basel, Basel, Switzerland. [7]Department of Pharmacology, Weill Cornell Medicine, New York, New York. [8]Inselspital, Bern, Switzerland. [9]Bern Center for Precision Medicine, Bern, Switzerland.

alterations in pathways downstream of AR, and increased signaling through other signaling pathways allowing for AR independence (29). Despite some recent progress in developing new treatments for CRPC, average survival at this advanced disease stage is approximately 3 years (30). Determining the mechanisms behind ARSi resistance is essential to improve existing therapies and finding new potential drug targets.

To address this gap in knowledge, we investigated the role of m⁶A and METTL3 in the progression of prostate cancer, with a particular focus on its role in regulating AR signaling and the response to ARSi. We show that low levels of *METTL3* in patients are associated with clinical markers of CRPC, in particular dysregulation of AR signaling. Using m⁶A individual-nucleotide-resolution cross-linking and immunoprecipitation (miCLIP), we mapped which transcripts are marked by m⁶A, and then further examined how METTL3 knockdown alters expression at the level of transcript, translation, and protein. In comparing these cell line results with patient data, we find that low METTL3 consistently increases expression of extracellular matrix genes. Furthermore, we examined the relationship between METTL3 and AR signaling and show that while knockdown of METTL3 has no effect on AR response genes, it does render the cells resistant to ARSi in an AR-independent manner that is driven by the upregulation of *NR5A2*. Overall, these findings support a new model for m⁶A function in affecting therapeutic sensitivity to ARSi, and suggest that patients with low levels of *METTL3* expression may not demonstrate an optimal response from ARSi.

Materials and Methods

Cell lines

LNCaP cells (male, ATCC, RRID: CVCL_1379) were maintained in RPMI medium (Gibco, A1049101), supplemented with 10% FBS (Gibco, 10270106) and 1% penicillin–streptomycin (Gibco, 11548876) on poly-L-lysine–coated plates. RWPE cells (male, ATCC, RRID: CVCL_3791) were maintained in Keratinocyte Serum Free Medium (Gibco, 17005075) supplemented with bovine pituitary extract and human recombinant EGF (included) and 1% penicillin–streptomycin (Gibco, 11548876). HEK293T cells (female, ATCC, RRID: CVCL_0063) and DU145 cells (male, ATCC, RRID: CVCL_0105) were maintained in DMEM (Gibco, 31966021), supplemented with 10% FBS and 1% penicillin–streptomycin. All cell lines were grown at 37°C with 5% CO₂. All cell lines were authenticated by short-tandem repeat analysis and regularly tested for mycoplasma.

miCLIP

Total RNA from LNCaP and RWPE cells was isolated with TRIzol according to the manufacturer instructions. PolyA⁺ mRNA was isolated using the PolyATtract mRNA Isolation System (Promega, Z5210). Twenty microgram of mRNA was used as input for miCLIP following the previously reported protocol (31) and an m⁶A antibody from Abcam (ab151230; RRID: AB_2753144). In parallel, total mRNA was subjected to library preparation using the Illumina library preparation protocol. Final libraries were sequencing on an Illumina HiSeq2500 generating 50 bp paired-end reads at the Weill Cornell Medicine Epigenetic Core facility.

Generation of inducible knockdown lines

Tet-pLKO-puro was a gift from Dmitri Wiederschain (Addgene plasmid # 21915; http://n2t.net/addgene:21915; RRID: Addgene_21915). Tet-pLKO-puro was digested with AgeI and EcoRI and ligated with annealed oligos (Supplementary Table S1). Lentivirus was pro-

duced in HEK293T cells by transfection with the pLKO constructs, and subsequent virus-containing media were used to transduce LNCaP cells. Three days after transduction, the cells were subjected to puromycin selection (1 μg/mL).

RNA sequencing and ribosome footprint profiling

For paired RNA and ribosome profiling (Ribo-seq) experiments, cells (∼15 × 10⁶) were incubated with 100 μg/mL cycloheximide for 5 minutes at 37°C. Cells were then trypsinized, pelleted, and the pellets washed twice with ice-cold PBS containing 100 μg/mL cycloheximide. An aliquot was set aside for confirmation of knockdown by Western blot, and the remaining cells were resuspended in 425 μL of hypotonic buffer [5 mmol/L Tris-HCl (pH 7.5), 2.5 mmol/L MgCl2, 1.5 mmol/L KCl, and 1× Halt protease inhibitor cocktail (Thermo Fisher Scientific, 78410)], followed by the addition of 50 μg cycloheximide, 1 μL of 1M DTT, and 100 units of RNAse Inhibitor (Thermo Fisher Scientific, N8080119). The pellet was vortexed, and 25 μL 10% Triton X-100 and 25 μL 10% sodium deoxycholate were added then followed by another vortex. The lysates were then cleared by spinning at 16,000 × g for 8 minutes at 4°C. The lysate was diluted 1:10, and optical density (OD) at 260 nm was determined using a Nanodrop spectrophotometer.

Ribosome footprinting was based on the manufacturer's instructions for the TruSeq Ribo Profile (Mammalian) Library Prep Kit (Illumina, discontinued). Briefly, lysates were normalized to OD of 30 and a volume of 200 μL. Then, 3 μL of RNAse I (Ambion, AM2294) was added, and the samples were incubated for 45 minutes at room temperature with shaking. Ten microliter of SUPERase•In was added to stop the reaction. Ribosome-bound RNA fragments were purified on MicroSpin S-400 HR Columns (Cytiva, 27-5140-01) followed by cleanup with the RNA Clean & Concentrator-25 kit. rRNA was removed using the NEBNext rRNA Depletion Kit (NEB, E6310), and 28 to 30 bp footprints were purified on a 15% polyacrylamide TBE/Urea gel. Ribo-seq libraries were then prepared with the purified footprints and the SMARTer Small RNA-Seq Kit (Takara, 635029) following the manufacturer's instructions.

RNA was extracted from either 100 μL of ribosome footprinting lysate with the RNA Clean and Concentrator-25 kit (Zymo, R1017), or directly from cells using the RNeasy Mini Kit (QIAGEN, 74106), and genomic DNA was removed using the DNA-free kit (Ambion, AM1906). RNA quality was assessed with a BioAnalyzer and quantity on a Qubit fluorometer. RNA sequencing (RNA-seq) libraries were prepared using 1 μg of RNA and the NEBNext Ultra II RNA Library Prep Kit (NEB, E7775) with rRNA depletion following the manufacturer's instructions.

All libraries were sequenced on an Illumina NextSeq generating 75-bp single-end reads at University of Basel Visceral Surgery and Precision Medicine Research Laboratory.

Bioinformatics analysis of sequencing data
miCLIP

Cross-linking–induced mutation sites were identified in miCLIP datasets as described previously (31). Individual m⁶A sites were subjected to metagene analysis using MetaPlotR (32). These identified sites were further filtered only reporting those sites that had greater than one cross-linking–induced mutation (m ≥ 2) and those that mapped to an A residue to generate Supplementary Data S1.

RNA-seq

Sequence reads were aligned to the human reference genome GRCh37 by STAR (RRID:SCR_004463) using the two-pass approach (33). Transcript quantification was performed using RSEM

(RRID:SCR_013027; ref. 34). Genes without >10 counts in at least 2 samples were discarded. Counts were normalized using the median of ratios method from the DESeq2 (RRID:SCR_000154) package in R version 3.6.1 (R Core Team (2019). R: A language and environment for statistical computing. R Foundation for Statistical Computing, Vienna, Austria (URL https://www.R-project.org/). Differential expression analysis was performed using the Wald test in DESeq2 (35).

Ribo-sequencing

Sequence reads were aligned as for RNA-seq, using STAR, but with the options—"winAnchorMultimapNmax 200 –seedSearchStartLmax 15 –outFilterMultimapNmax 20"—to improve mapping of short Ribo-seq reads. Differential analysis of ribosome loading was performed using Riborex, which uses generalized linear models and the DESeq2 normalization framework to identify genes showing altered translation between sample groups (36).

Drug treatments

For all drug treatments, cells were pretreated with 200 ng/mL doxycycline for 96 hours to induce shRNAs. For dihydroxytestosterone (DHT) stimulation experiments, cells were starved of hormone for 48 hours in phenol red–free RPMI media (Gibco, 11-835-030) with 10% charcoal-stripped FBS (Gibco, A3382101) and then treated with 10 nmol/L dihydrotestosterone or 10 µmol/L ENZ for 24 hours.

For Incucyte experiments, cells were treated with doxycycline for 96 hours and then plated in a 96-well plate, 5,000 cells per well ($n = 8$ per condition). Cell confluency was determined using the Incucyte S3 instrument and the Incucyte S3 2018B software. Values were calculated as fold change in confluency as compared with vehicle-treated controls.

Double knockdown experiments

Inducible shRNA lines were pretreated with doxycycline for 72 hours and then plated in a 96-well plate, 10,000 cells per well while continuing doxycycline treatment. The next morning, cells were transfected with SMARTpool (Dharmacon) pools of four siRNAs targeting AR (L-003400-00-0005), NR5A2 (L-003430-00-0005), or a nontargeting pool (D-001810-10-05). That evening (8 hours after transfection), cells were treated with media containing 10 µmol/L ENZ or DMSO ($n = 4$ per condition) and placed in the Incucyte.

Proteomics

Inducible shRNA lines were treated with 200 ng/mL doxycycline for 96 hours. Cells were scraped directly in lysis buffer (8 mol/L urea, 100 mmol/L Tris pH8, plus protease inhibitors) and lysed with sonication for 1 minute on ice with 10-second intervals. The supernatant was reduced, alkylated, and precipitated overnight. The pellet was resuspended in 8 mol/L urea/50 mmol/L Tris, pH 8, and protein concentration was determined with Qubit Protein Assay (Invitrogen).

Ten micrograms of protein were digested with LysC for 2 hours at 37°C followed by Trypsin at room temperature overnight. Eight hundred nanograms of digests were loaded in random order onto a precolumn (C18 PepMap 100, 5 µm, 100 A, 300 µm i.d. × 5 mm length, Thermo Fisher Scientific, 160454) at a flow rate of 50 µL/min with solvent C (0.05% TFA in water/acetonitrile 98:2).

After loading, peptides were eluted in back flush mode onto a home-packed analytical Nano-column (Reprosil Pur C18-AQ, 1.9 µm, 120 A, 0.075 mm i.d. × 500 mm length) using an acetonitrile gradient of 5% to 40% solvent B (0.1% formic acid in water/acetonitrile 4,9:95) in 180 minutes at a flow rate of 250 nL/min. The column effluent was directly coupled to a Fusion LUMOS mass spectrometer (Thermo Fischer Scientific) via a nanospray ESI source.

Data acquisition was made in data-dependent mode with precursor ion scans recorded in the orbitrap with resolution of 120,000 (at $m/z = 250$) parallel to top speed fragment spectra of the most intense precursor ions in the Linear trap for a cycle time of 3 seconds maximum.

The mass spectrometry data were processed with MaxQuant (ref. 37; version 1.6.1.0) against the Swissprot Homo Sapiens database (ref. 38; release February 2019). The initial precursor mass tolerance was set to 10 ppm, and that of the fragment peaks to 0.4 Da. Enzyme specificity was set to strict trypsin, and a maximum of three missed cleavages were allowed. Carbamidomethylation on cysteine was set as a fixed modification, methionine oxidation, and protein N-terminal acetylation as variable modifications. The same fraction number was given to all replicates of a group, but each group was given a fraction number differing by 3, so that match between runs was prevented between the different groups.

Protein intensities are reported as MaxQuant's Label Free Quantification (LFQ) values, as well as iTop3 (39) values (sum of the intensities of the three most intense peptides); for the latter, variance stabilization (40) was used for the peptide normalization, and missing peptide intensities, if at least two evidences exist in a group, were imputed by drawing values from a Gaussian distribution of width 0.3 centered at the sample distribution mean minus 1.8x the sample SD. Imputation at protein level for both iTop3 and LFQ was performed if there were at least two measured intensities in at least one group of replicates; missing values in this case were drawn from a Gaussian distribution of width 0.3 centered at the sample distribution mean minus 2.5× the sample SD. Differential expression tests were performed using empirical Bayes (moderated t test) implemented in the R limma (RRID:SCR_010943) package (41). The Benjamini and Hochberg (42) method was further applied to correct for multiple testing.

Immumoblotting

Cells were lysed in RIPA buffer with protease inhibitors, resolved on 4% to 15% Mini-Protean TGX gels (BioRad, 456-1084), and transferred to nitrocellulose membranes using the iBlot2 system (Thermo Fisher Scientific, IB23001). Blots were blocked for 1 hour at room temperature and then probed with primary antibodies against METTL3 (Cell Signaling Technology, 96391; RRID: AB_2800261), KIF5C (Abcam, ab193352), GAPDH (Millipore, AB2302; RRID: AB_10615768), IFIT3 (Santa Cruz Biotechnology, sc-393512; RRID: AB_2857847), STAT1 (Cell Signaling Technology, 14994; RRID: AB_2737027), phospho-STAT1 (Cell Signaling Technology, 7649; RRID:AB_10950970), or beta-actin (Abcam, ab6276; RRID: AB_2223210) overnight in 5% milk or BSA (all Cell Signaling Technology antibodies) in TBST at 4°C. After four washes, blots were incubated with IRDye secondary antibodies (LI-COR: 926-68075, RRID:AB_10974977; 926-32211, RRID:AB_621843; 926-32210, RRID:AB_621842) in 5% milk for 1 hour at room temperature. After four washes, blots were visualized on a LI-COR Odyssey Infrared Imaging System.

m⁶A immunoprecipitation

Total RNA was isolated with TRIzol according to the manufacturer's instructions, and PolyA+ mRNA was isolated using Dynabeads Oligo(dT)$_{25}$ (Invitrogen, 61002), and genomic DNA was removed using the DNA-free kit (Ambion, AM1906). 3.5 µg of mRNA was fragmented (Invitrogen, AM8740), along with 4 pmol each of positive and negative control mRNAs (New England Biolabs, E1610S). Ten

percent of each sample was saved as input, and the remainder was brought up to 500 μL with IP buffer (50 mmol/L Tris, pH 7.4, 150 mmol/L NaCl, 0.5% NP-40) and coupled to 2 μL of m⁶A antibody (Abcam, ab151230; RRID: AB_2753144) at 4°C for 2 hours. Antibody-bound mRNA was precipitated with 50 μL of Protein AG beads (Thermo Fisher Scientific, 88803) at 4°C for 1 hour. Beads were then washed 5 times in IP buffer, and RNA was eluted in RNA Binding Buffer and purified using clean up columns (Zymo, R1013). RNA was reverse transcribed using random primers and SuperScript IV Reverse Transcriptase (Invitrogen, 18090010). The input fraction was split into two in order to run in parallel a no reverse transcriptase control to assess for any potential amplification of contaminating genomic DNA.

qPCR

RNA was extracted directly from cells using the RNeasy Mini Kit with an on column DNAse treatment. RNA was reverse transcribed using the FIREScript RT cDNA kit and random primers (Solis Biodyne, 06-15-00200) according to the manufacturer's instructions. Quantitative real-time PCR was performed on the ViiA 7 system (Applied Biosystems) using HOT FIREPol EvaGreen qPCR mix (Solis Biodyne, 08-24-00020) following the manufacturer's instruction. Primer sequences are listed in Supplementary Table S1. All quantitative real-time PCR assays were carried out using three technical replicates. Relative quantification of quantitative real-time PCR data used GAPDH, ACTB, and HMBS as housekeeping genes.

IFN stimulation

Cells were treated with 200 units/mL of recombinant IFNα (Abcam, ab48750) for between 4 and 24 hours before Western blot analysis.

Materials availability

Inducible shRNA plasmids generated in this study have been deposited to Addgene (Plasmid #:162984, RRID:Addgene_162984; 162985, RRID:Addgene_162985; and 163017, RRID:Addgene_163017).

Cell lines generated in this study are available from the Lead Contact with a completed Materials Transfer Agreement.

Data and code availability

The miCLIP, RNA, and Ribo-Seq data discussed in this publication have been deposited in NCBI's Gene Expression Omnibus (70) and are accessible through GEO Series accession number GSE161304 (https://www.ncbi.nlm.nih.gov/geo/query/acc.cgi?acc=GSE161304).

Raw images of blots in the paper have been deposited to Mendeley data: http://dx.doi.org/10.17632/xv2vzc8pzz.1.

The mass spectrometry proteomics data have been deposited to the ProteomeXchange Consortium (http://proteomecentral.proteomexchange.org) via the PRIDE partner repository (71) with the dataset identifier PXD022348.

Results

Low METTL3 expression is associated with advanced prostate cancer

Given the ability of m⁶A to influence gene expression, we asked whether m⁶A affects prostate cancer progression. To determine if changes in m⁶A might contribute to prostate cancer in patients, we assessed if the expression of the methyltransferase m⁶A "writer" complex members (METTL3, METTL14, WTAP, VIRMA, ZC3H13, and RBM15), the m⁶A "eraser" ALKBH5, or the m⁶A "reader" proteins (YTHDF1, YTHDF2, and YTHDF3) is related to any clinical parameters in advanced prostate cancer. In a recent precision oncology

study, we reported on 430 men with CRPC (43). We subset these patients based on the relative expression levels of each member into low (z-score of less than -1) and high (z-score of greater than 1) groups. We then assessed whether these groups demonstrated low AR signaling or high neuroendocrine scores, both important measures for a lack of response to antiandrogen therapy (44).

Although previous studies suggested that METTL3 expression is higher in primary prostate cancer as compared with benign prostate tissue (26, 27), our examination of the expression of METTL3 in metastatic prostate cancer samples revealed the opposite phenomena, that decreased METTL3 is associated with the most aggressive subclass of advanced prostate disease. In this cohort of 430 men with metastatic CRPC, we observed that those with lower levels of METTL3 demonstrated significantly disrupted AR signaling ($P = 0.0011$; **Fig. 1A**), and significantly increased expression of genes associated with neuroendocrine progression ($P = 0.0214$; **Fig. 1B**). This association between low expression and low AR score also held true for METTL14 ($P = 0.0002$), WTAP ($P = 0.0002$), VIRMA ($P = 3.79E-06$), ALKBH5 ($P = 0.0034$), YTHDF1 ($P = 0.0323$), YTHDF2 ($P = 0.0024$), and YTHDF3 ($P = 0.0096$; Supplementary Fig. S1A). In contrast, ZC3H13 expression did not show a significant association with AR score (Supplementary Fig. S1A); however, it was the only other gene besides METTL3 to have a significant association with NEPC score, albeit in the opposite direction ($P = 0.0433$; Supplementary Fig. S1B).

In this same group of patients, those with lower METTL3 expression were also more likely to have primary tumors with higher Gleason scores (8 and above) than those with high METTL3 expression ($P = 0.0111$; **Fig. 1C**). None of the other methyltransferase complex members, reader proteins, or ALKBH5 showed any association with Gleason score (Supplementary Fig. S1C). Given these data, and its known role as the catalytic subunit of the "writer" complex, we chose to focus further investigations on METTL3.

To begin to understand the mechanistic links between m⁶A and these signifiers of aggressive CRPC, we asked what genes and/or pathways are associated with differential METTL3 expression in prostate cancer. To begin to address this question, we took the same cohort of metastatic patient samples categorized into METTL3-high and METTL3-low groups, and looked for genes over- or underexpressed in one group versus the other. This analysis identified 2,692 genes with significantly reduced expression in the METTL3-low group and 2,081 genes with significantly increased expression. Gene set enrichment analysis of these genes demonstrates that those that correlate positively with METTL3 expression mainly involve genes associated with transcription and mRNA processing (**Fig. 1D**). On the other hand, gene sets that display a negative correlation with METTL3 expression include many pathways implicated in aggressive metastatic disease, including complement and coagulation pathways, epithelial–mesenchymal transition, regulation of the extracellular matrix, and drug metabolism (**Fig. 1D**).

Mapping m⁶A in prostate cancer

Given that our above analysis relies solely on correlations in gene expression within a diverse group of patient samples, we aimed to more thoroughly define the role of m⁶A methylation in the regulation of prostate cancer gene expression. As a first step, we sought to generate the first epitranscriptomic maps of m⁶A in prostate cancer. Using miCLIP (31), we mapped the location of m⁶A at a single-nucleotide resolution throughout the entire transcriptomes of both the AR-sensitive adenocarcinoma LNCaP and in the benign RWPE cell line and identified over 18,000 methylated residues in 6,653 transcripts. Similar to previously reported m⁶A maps generated in other cell lines
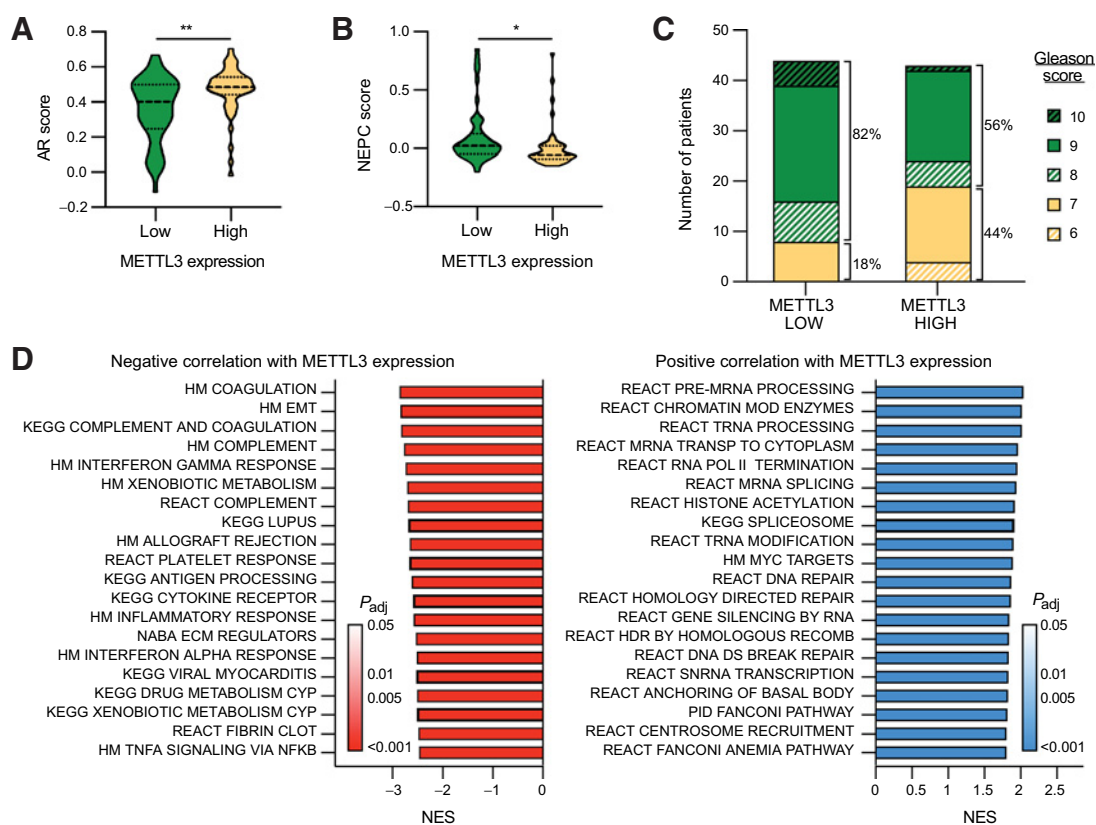
Figure 1.
Low *METTL3* expression is associated with advanced-stage disease. CRPC samples (43) were grouped based on *METTL3* expression: high, z-score > 1, n = 50; low, z-score < −1, n = 49. **A,** AR score in *METTL3*-high versus -low samples. Median and quartiles are indicated with a dotted line, P = 0.0011 as determined by t test. **B,** NEPC score in *METTL3*-high versus -low samples. Median and quartiles are indicated with a dotted line, P = 0.0214 as determined by t test. **C,** Gleason score in *METTL3*-high versus -low samples. P = 0.0111 as determined by Fisher exact test between samples with Gleason 6–7 and Gleason 8+ scores. **D,** Gene set enrichment analysis of genes differentially expressed in in *METTL3*-high versus -low samples. Genes were ranked according to the log of the Benjamini and Hochberg–adjusted P value as determined by t test. Shown are the top 20 results in either direction.

and tissues, the majority of m6A sites identified in both cell lines were in the 3′ UTR, particularly in the vicinity of the stop codon (**Fig. 2A**). Furthermore, the sequence context surrounding the methylation sites was also consistent with the previously reported DRACH motifs (D = A/G/U, R = A/G, H = A/C/U; **Fig. 2B**; refs. 14, 45).

In both lines, the 70% to 85% of transcripts had only one or two annotated sites; however, 1% to 2% of the transcripts had 10 or more (Supplementary Data S1 and S2). In both lines, the noncoding RNA *MALAT1* was the most highly methylated with 84 annotated sites in LNCaP and 69 in RWPE. Examination of the association between the total of number of annotated sites identified per transcript and its expression shows that although there is some bias toward highly expressed genes having more total sites (due to inherent biases in IP-based protocols), expression is not the sole driver of the differences seen (Supplementary Fig. S2A). Furthermore, there was no correlation between the number of annotated m6A sites and the transcript length (Supplementary Fig. S2B).

To determine the cellular pathways that m6A might influence in prostate cancer, we interrogated the miCLIP data using gene set enrichment analysis to identify pathways enriched in the transcripts that exhibited higher number of annotated m6A sites. This analysis implicated m6A in regulating mRNAs that encode pathways related to cell adhesion and the extracellular matrix in both cell lines (**Fig. 2C**).

Remarkably, this enrichment is similar to the gene expression changes linked to low *METTL3* expression based on examination of the patient samples (see **Fig. 1D**). In particular of the transcripts differentially expressed between the *METTL3*-high and -low groups, 1,430 and 684 exhibited at least one annotated m6A site in LNCaP or RWPE cells, respectively (Supplementary Fig. S2C). In addition, this analysis identified AR-regulated genes as also having a high number of annotated m6A sites in LNCaP cells. In particular, AR signature genes including *KLK2, KLK3, NKX3–1*, and even *AR* itself all had greater than 10 sites (**Fig. 2D**).

We further characterized the methylation status of transcripts by not only the number of annotated sites on a given transcript, but also a relative measurement of the amount of m6A at a given site. To do so, we normalized the amount of fragmented RNA immunoprecipitated using the m6A antibody from each individual site to the library size (uTPM), and overall expression of that transcript (Supplementary Fig. S2D). As in Supplementary Fig. SS2A, we see a correlation between the amount of immunoprecipitated RNA and the expression of the transcript. Nonetheless, we can also identify distinct subsets of transcripts which have relatively high or low levels of methylation given their expression. In both cell lines, this analysis again identified AR pathway genes as having high levels of methylation, whereas ribosomal and translation pathways had low levels of
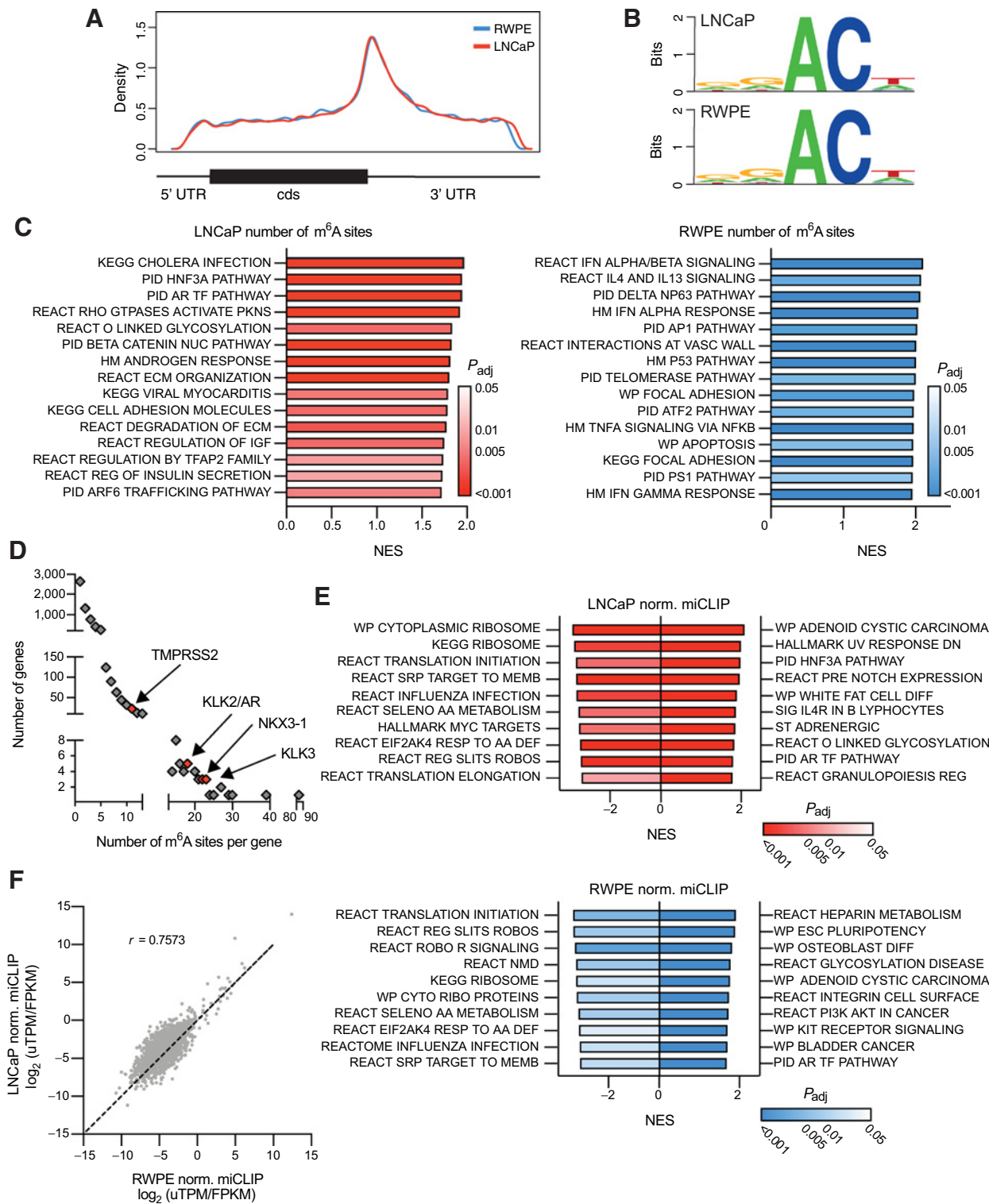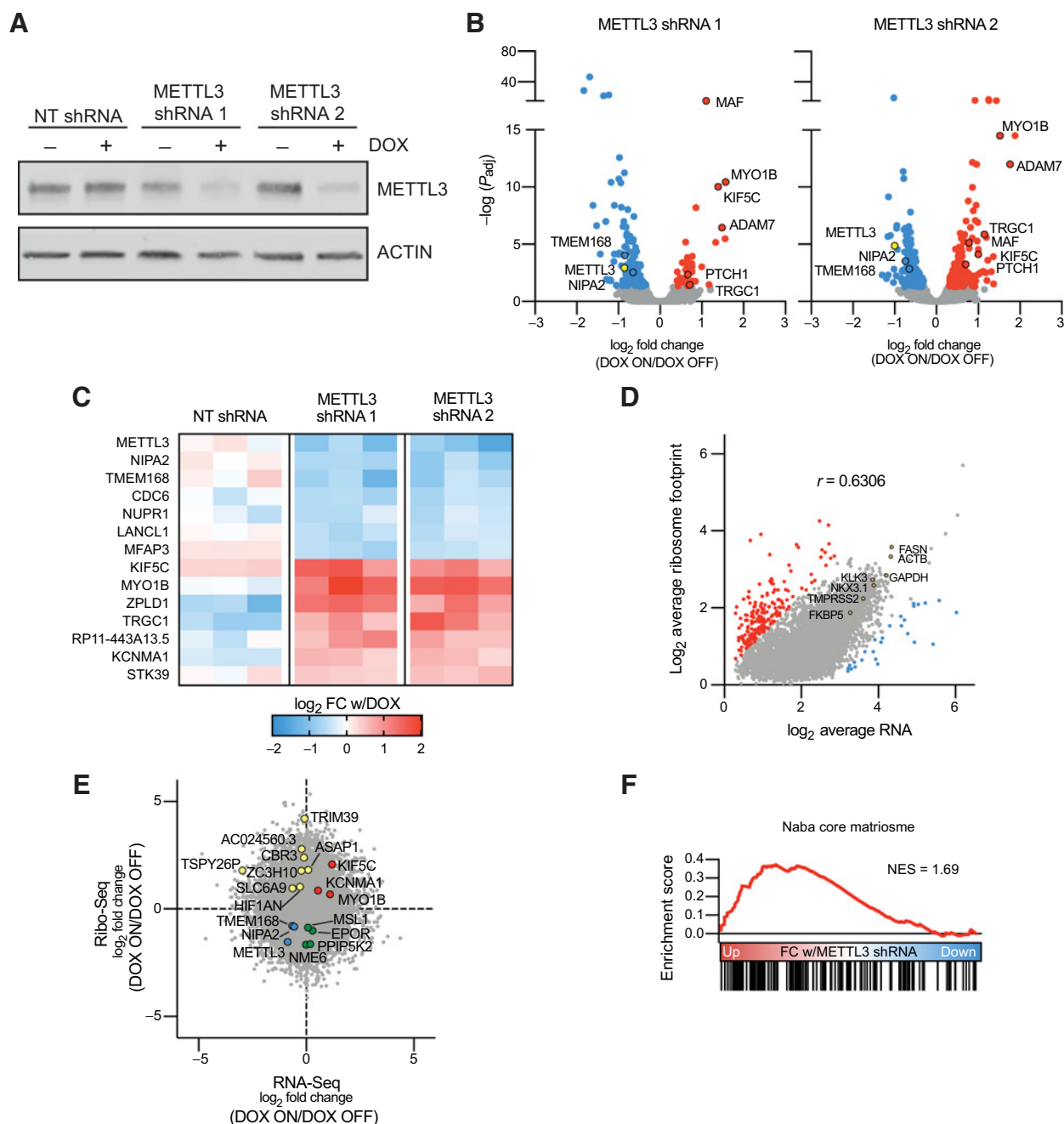
Figure 2.
Mapping genes methylated with m⁶A in prostate cancer. m⁶A was mapped in LNCaP and RWPE cell lines using miCLIP. **A,** Metagene plot of the distribution of m⁶A residues along the transcript in both cell lines. **B,** Consensus sequence surrounding m⁶A sites identified in both cell lines generated with WebLogo. **C,** Gene set enrichment analysis of genes ranked by the number of m⁶A sites. Shown are the top 15 gene sets. **D,** AR signature genes ($n = 30$; ref. 72) are significantly ($P = 0.0004$) enriched in m⁶A sites (>10 sites) as determined by Fisher exact test. **E,** Gene set enrichment analysis of genes ranked by the total normalized miCLIP unique tags per million for a given transcript. **F,** Comparing the normalized miCLIP unique tags per million per transcript in genes which are similarly expressed (<10-fold difference) between the LNCaP and RWPE cell lines.

methylation relative to the expression levels of those transcripts (**Fig. 2E**) in agreement with results from other human cell lines (11).

Comparisons of methylation sites between the two lines are of course heavily biased by the highly divergent transcriptomes between LNCaP and RWPE cells. However, upon limiting the analysis to transcripts with less than a 10-fold difference in expression between the two lines, we find a strong correlation between the amount of m⁶A (Pearson $r = 0.7573$; **Fig. 2F**). In particular, upon comparing the
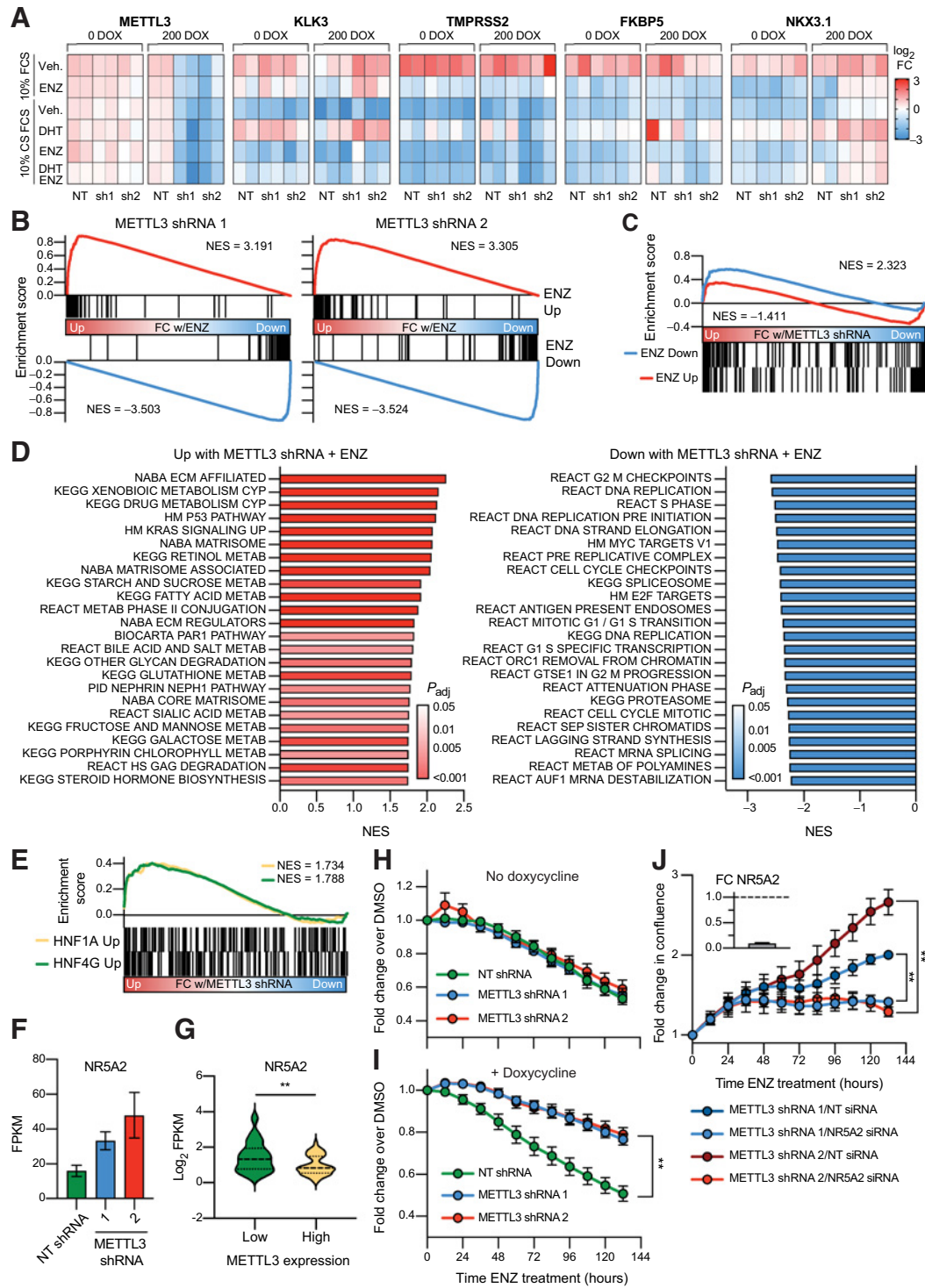

Figure 3.
Knockdown of *METTL3* in prostate cancer alters gene expression and translation. **A,** Generation of LNCaP cell lines with two doxycycline-inducible shRNAs targeting *METTL3*, or a nontargeting shRNA targeting *GFP*. Cells were treated with doxycycline for 96 hours followed by Western blot analysis for METTL3. **B,** Significantly (adjusted *P* value < 0.05) differentially expressed genes with *METTL3* knockdown in the two inducible shRNA lines (*n* = 3). Common genes between the two shRNA lines are highlighted with a black border. **C,** Six transcripts are significantly downregulated and seven transcripts are significantly upregulated with *METTL3* knockdown in both shRNA lines, but not the nontargeting line (*n* = 3). **D,** Correlation (Pearson *r* = 0.6306, *P* < 1E-15) between the average mRNA (*n* = 6) and ribosome footprint (*n* = 4) from the *METTL3* shRNA lines without doxycycline. Outliers with extreme high (red) and low (blue) TE (Ribo/RNA) were calculated using ROUT analysis (*Q* = 1%). **E,** Riborex analysis of Ribo-seq data identifies genes with changes in TE independent of changes in mRNA expression. Shown is the fold change with doxycycline treatment in both *METTL3* shRNAs combined as determined by DESeq2 (RNA-seq, *n* = 12; Ribo-seq, *n* = 10). **F,** Gene set enrichment analysis of genes ranked by the fold change in TE with *METTL3* knockdown as determined by Riborex.
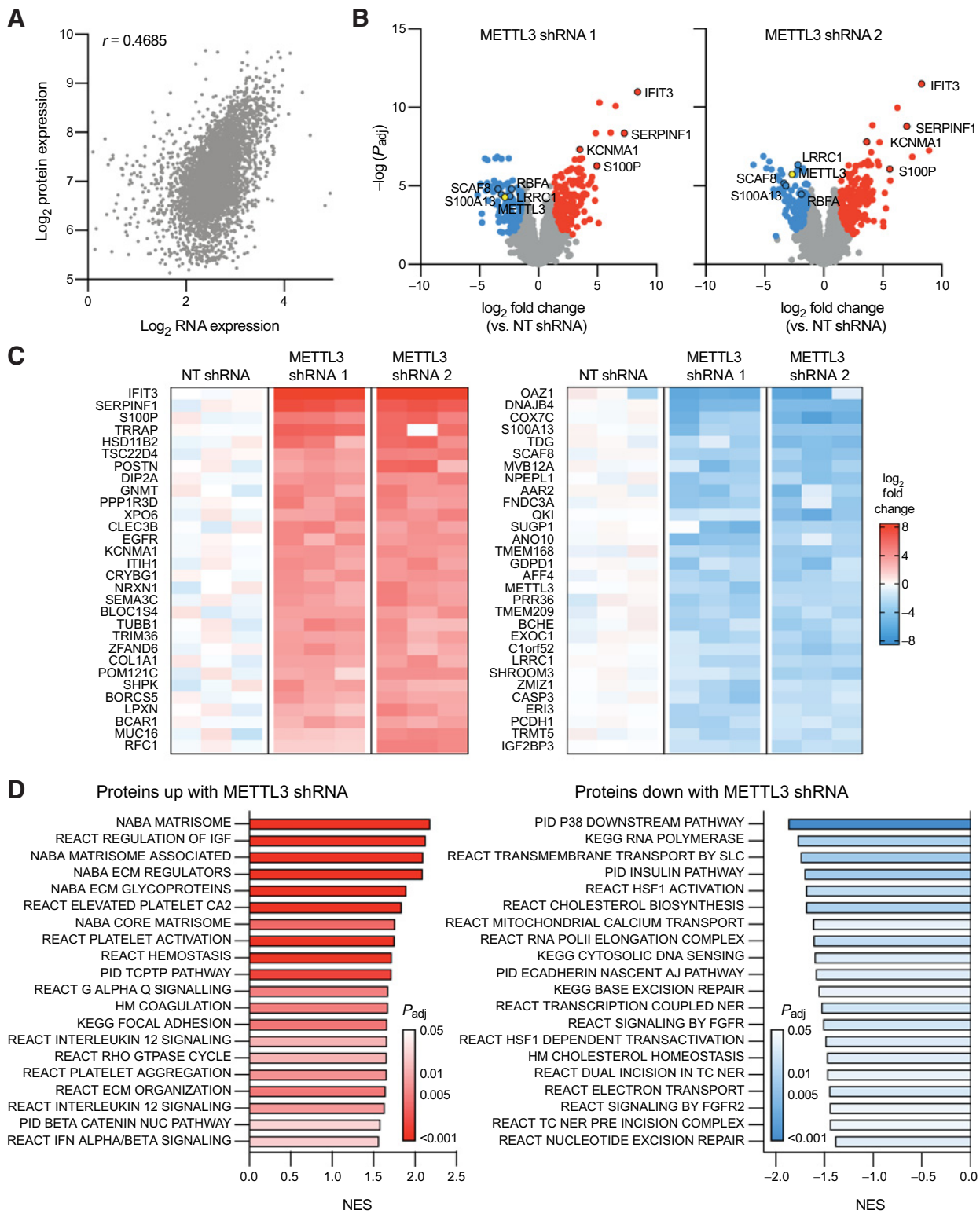
Figure 4.
Knockdown of *METTL3* in prostate cancer alters protein expression. **A,** Correlation (Spearman $\rho = 0.4685$, $P < 1E\text{-}15$) between the average mRNA expression ($n = 3$) and protein expression ($n = 3$) as determined by shotgun proteomics in the NT shRNA line. **B,** Significantly (adjusted P value < 0.05) differentially expressed proteins with *METTL3* knockdown in the two inducible shRNA lines as compared with the NT shRNA line ($n = 3$ for each shRNA). Common highly differentially expressed proteins between the two shRNA lines are highlighted with a black border. **C,** The top 60 differentially expressed proteins seen with *METTL3* knockdown in both shRNA lines as compared with the NT control ($n = 3$ for each shRNA). **D,** Gene set enrichment analysis of proteins differentially expressed with *METTL3* knockdown. Proteins were ranked according to the log of the adjusted P value as determined by t test. Shown are the top 20 results in either direction.

Figure 5.

METTL3 knockdown leads to the induction of a gene signature linked to castration resistance and renders the cells resistant to enzalutamide in an AR-independent manner. **A,** Change in expression of AR target genes with *METTL3* knockdown (±doxycycline) and in response to AR stimulation (10 nmol/L DHT) or inhibition (10 μmol/L ENZ). Expression was measured via qPCR ($n = 2$) and is displayed as the fold change with treatment per gene and experiment. **B,** RNA-seq analysis of *METTL3* knockdown lines treated with ENZ demonstrates no change in the repression or activation of known ENZ target genes by gene set enrichment analysis. Genes were ranked according to the fold change ENZ versus vehicle as determined by DESeq2. ENZ up and down gene lists contain the common differentially expressed genes from two published RNA-seq experiments (GSE110903 and GSE147250). **C,** Some ENZ-responsive genes show differential expression with *METTL3* knockdown. (*Continued on the following page.*)

amount of methylation at m^{6}A sites common to both cell lines, we found a striking concordance between the levels in LNCaP and RWPE cells (Pearson $r = 0.8666$; Supplementary Fig. S2E).

METTL3 regulation of gene expression and translation

Although the miCLIP analysis identified many highly methylated transcripts with known functional relevance in prostate cancer, in particular *AR* and its downstream target genes, it remains to be seen whether methylation of these transcripts plays a specific role in their regulation, and further whether this regulation is at the level of transcript stability and/or TE. To address this, we generated LNCaP cell lines infected with drug-inducible shRNAs targeting *METTL3*. With these lines, we were able to precisely and coordinately manipulate both the timing and extent of reduction of *METTL3* expression. We demonstrated a robust knockdown of METTL3 expression after 96 hours of doxycycline treatment (**Fig. 3A**) as compared with a control nontargeting shRNA against *GFP*. Further the METTL3 knockdown is reversible after 144 hours of doxycycline washout (Supplementary Fig. S3A).

Using these inducible lines, we measured changes in both expression and TE by means of tandem RNA-seq and Ribo-seq. RNA-seq analysis demonstrated relatively modest changes in gene expression with *METTL3* knockdown. With either *METTL3* shRNA, we found 187 and 337 significantly (FDR < 0.05) differentially expressed genes between the doxycycline on and off conditions (**Fig. 3B**). However, we also identified 508 significant gene expression changes in the nontargeting line in response to doxycycline, including three which were also significant in both our *METTL3* shRNA lines (Supplementary Fig. S3B). This strategy allowed us to specifically identify six down- and seven upregulated transcripts (**Fig. 3C**) which were significantly regulated in two different *METTL3* knockdown lines, after considering nonspecific effects of doxycycline treatment or shRNA induction. Of these 13 transcripts, 7 were identified in our previous miCLIP experiments to have at least one m^{6}A mark in LNCaP cells (Supplementary Data S1).

To determine if these changes persisted at the protein level, we validated one of the most upregulated transcripts *KIF5C*. We confirmed persistent KIF5C upregulation at the protein level after only 72 hours of doxycycline treatment (Supplementary Fig. S3C). *KIF5C* is further of interest in that in metastatic prostate cancer samples its expression is highly correlated with AR signaling (Spearman's $\rho = 0.56$; Supplementary Fig. S3D). Given that expression of *KIF5C* itself is not regulated by AR signaling in LNCaP cells (fold change < 2 with DHT or ENZ; Supplementary Fig. S3E), it remains to be seen whether KIF5C operates upstream of AR, or if it plays some other role in prostate cancer progression.

Similar to published Ribo-seq results from other cell lines and tissues (46), ribosome footprinting read counts generally correlated with mRNA expression in LNCaP cells (Pearson $r = 0.6306$; **Fig. 3D**).

Among the most highly expressed and ribosome-bound transcripts are the housekeeping genes *GAPDH* and *ACTB*, and the known AR targets *KLK3*, *FASN*, *NKX3.1*, *FKBP5*, and *TMPRSS2*. We did, however, also identify 225 transcripts that were outliers (ROUT analysis, $Q = 1\%$) with ribosome footprints that do not correlate with mRNA expression. Eight of the 27 transcripts with exceptionally low TE are mitochondrial genes which are known to be inefficiently captured with standard ribosome footprinting protocols (47). Other gene sets with generally low TE include ribosomal proteins and pathways involved in translation (similar to results from proteogenomic studies demonstrating a low correlation between transcript and protein for ribosomal proteins in human tumors; refs. 48–50), whereas those with high TE are predominated by extracellular matrix proteins in particular collagens (Supplementary Fig. S3F).

We then utilized Riborex (36) analysis to identify genes with significant changes in TE independent of any changes in mRNA expression. This analysis further identified 15 and 6 genes with a significant (FDR < 0.1) increase or decrease in TE with *METTL3* knockdown in both of the inducible shRNA lines (**Fig. 3E**), of which 6 were have at least one m^{6}A mark in LNCaP cells (Supplementary Data S1). Gene set enrichment analysis demonstrated that the TE of transcripts encoding extracellular matrix proteins is increased with *METTL3* knockdown (**Fig. 3F**).

METTL3 regulation of protein expression

Given the changes we detected in TE with *METTL3* knockdown, we then wanted to understand how these changes are reflected in protein abundance. Therefore, we conducted shot-gun proteomics using the same inducible *METTL3* shRNA lines in order to get an unbiased and quantitative picture of the entire proteome. Protein expression generally correlated with mRNA expression (Spearman $\rho = 0.443–0.469$) in line with recent results describing paired RNA-seq and proteomics in prostate cancer patient samples (**Fig. 4A**; ref. 6).

We identified 527 and 537 significantly differentially expressed (FDR adj *P* value < 0.05, FC > 2) proteins in either *METTL3* shRNA line as compared with the nontargeting shRNA line (**Fig. 4B**). Similar to our Ribo-seq results, we also observed much larger fold changes at the protein level (>15-fold) than we had seen at the level of expression (2–4-fold, **Fig. 3B**). Unfortunately, only one of the transcripts with significant changes in TE was detected in our proteomics experiment, thus precluding a thorough comparison between the two methods; nonetheless, this protein (CBR3) was upregulated in both cell lines after *METTL3* knockdown. In total, 182 proteins significantly upregulated in both *METTL3* shRNA lines, whereas 109 proteins were significantly downregulated (**Fig. 4C**, Supplementary Data S3), and of these, 160 have at least one m^{6}A mark (Supplementary Data S1). Previous studies have identified IFN signaling as being highly upregulated in response to *METTL3* knockdown (51, 52). Here, we

---

(*Continued.*) Ranking for gene set enrichment analysis was according to the combined fold change ENZ versus vehicle as determined by DESeq2 for both *METTL3* shRNA lines. **D,** Gene set enrichment analysis of genes differentially expressed with ENZ treatment and *METTL3* knockdown. Genes were ranked according to the combined Wald statistic from DESeq2 for both *METTL3* shRNA lines as compared with the NT shRNA. Shown are the top 24 results in either direction. **E,** *METTL3* knockdown with ENZ treatment induces the expression of HNF1A and HNF4G target genes. Genes were ranked according to the combined Wald statistic from DESeq2 for both *METTL3* shRNA lines. HNF target genes were taken from previously published overexpression experiments in LNCaP cells (GSE85559). **F,** NR5A2 is overexpressed with *METTL3* knockdown and ENZ treatment ($n = 3$, error bars = SEM) **G,** NR5A2 expression in *METTL3*-high versus -low samples (see **Fig. 1**). Median and quartiles are indicated with a dotted line, $P = 0.0034$ as determined by t test. **H,** In the absence of *METTL3* knockdown, the shRNA lines respond similarly to 10 μmol/L ENZ treatment ($n = 3$, error bars = SEM). **I,** Induction of *METTL3* knockdown renders the cells resistant to ENZ treatment ($n = 4$, error bars = SEM; sh1 $P = 0.0012$, sh2 $P = 0.0011$, as determined by t test). For both panels, shown is the change in cell confluency as compared with DMSO with time as measured via Incucyte imaging. **J,** Knockdown of *NR5A2* significantly reverses the ability of the *METTL3* knockdown cells to proliferate in the presence of 10 μmol/L ENZ ($n = 3$, error bars = SEM; sh1 $P = 0.001003$, sh2 $P = 0.001223$, as determined by t test). Plotted is the fold change in confluency compared with time zero. Sufficient *NR5A2* knockdown (91%) was confirmed in tandem by qPCR and is plotted in the top left as fold change over NT siRNA ($n = 3$).

---

identified an upregulation of the IFN-induced proteins IFIT1, IFIT2, and IFIT3, but not other IFN-induced proteins. This is likely due to the fact that LNCaP cells are unresponsive to IFN signaling (Supplementary Fig. S4) due to a silencing of JAK1 by biallelic inactivating mutations and epigenetic silencing in this line (53, 54).

Gene set enrichment analysis of the proteomics data revealed that downregulated proteins mainly included those associated with transcription and repair of DNA damage (**Fig. 4D**). Gene sets with upregulated proteins predominantly consisted of those involved in the composition and regulation of the extracellular matrix, coagulation, and cell adhesion. This is consistent with results seen in patients with low *METTL3* expression (**Fig. 1D**) and genes with high levels of m^{6}A in LNCaP cells (**Fig. 2D**).

METTL3 knockdown triggers AR independence

Recent work has demonstrated that the majority of the effects of m^{6}A are mediated through a reduction in transcript stability (16, 55). Given this, one would expect that we would see an increase in expression of the highly methylated AR pathways genes (**Fig. 2D**), and therefore AR signaling, with *METTL3* knockdown. In contrast, we see no change in the expression of these genes at the transcript (**Fig. 3C**) or protein level (**Fig. 4C**). Furthermore, the expectation of an increase in AR signaling with *METTL3* knockdown is inconsistent with the results we saw in the metastatic patient cohort where low levels of *METTL3* were associated with a lower AR score, indicating a disruption of AR signaling overall (**Fig. 1A**).

To resolve these contradictions, we decided to directly examine the response of the *METTL3* knockdown lines to treatment with ENZ (a potent AR ligand binding inhibitor), and/or stimulation with DHT. We then examined the changes in expression of known AR target genes (i.e., *KLK3, TMPRSS2, FKBP5*, and *NKX3*.1) by qPCR (**Fig. 5A**). In the absence of *METTL3* knockdown, all three cell lines responded similarly to the treatments. Further, with *METTL3* knockdown, we saw no change in the response of *KLK3, FKBP5*, and *TMPRSS2* to AR inhibition with ENZ or charcoal-stripped (hormone-free) media, nor to DHT stimulation. In contrast, we did see a significant reduction in the downregulation of *NKX3*.1 with *METTL3* knockdown and ENZ (sh1, $P = 0.0062$; sh2, $P = 0.0074$) or charcoal-stripped media (sh1, $P = 0.036$; sh2, $P = 0.044$) treatment. *NKX3*.1 is a prostate-specific homeobox gene that regulates normal prostate differentiation and suppresses prostate cancer initiation (56). The upregulation of *NKX3*.1 with DHT stimulation, however, remained unchanged (FC sh1 = 2.3, FC sh2 = 2.6, vs. FC NT = 3). As such, we concluded that *METTL3* knockdown does not alter AR signaling overall in LNCaP cells.

In order to get a global view of the response to *METTL3* knockdown and AR inhibition with ENZ, we analyzed changes in gene expression with RNA-seq. As expected, we again confirmed that *METTL3* knockdown did not change known AR signaling pathways, as most canonical ENZ-responsive genes responded as expected to the treatment (**Fig. 5B**). Nonetheless, we did identify some genes, which, similar to *NKX3*.1, demonstrated a reduction in the magnitude of their repression or activation with ENZ (**Fig. 5C**). For example, *MAML2* is downregulated 5.8-fold with ENZ and the NT shRNA, yet only 3.48- and 2.92-fold with the *METTL3* shRNAs (Supplementary Fig. S5A).

Overall 54 genes were significantly upregulated with both *METTL3* shRNAs and under ENZ treatment conditions, whereas 25 genes were significantly downregulated (FDR < 0.05, Supplementary Data S4). Of these 79 differentially expressed transcripts, 40 were identified as having at least one annotated m^{6}A site in our miCLIP analysis of LNCaP cells (see Supplementary Data S1). Importantly, the upregu-

lated genes included many which have been previously linked to ENZ resistance including *TMEFF2, ADAMTS1* (57), and *COL5A2* (58). Gene set enrichment analysis of genes which are differentially expressed with *METTL3* knockdown in response to ENZ again identified an enrichment in pathways related to extracellular matrix components (**Fig. 5D**), which is consistent with our above results in patient expression data (**Fig. 1D**), m^{6}A mapping (**Fig. 2C**), ribosome footprinting (**Fig. 3F**), and proteomics (**Fig. 4D**) analysis.

In addition, we also identified many pathways involved in the metabolism of drugs and other compounds that were significantly upregulated with *METTL3* knockdown, again consistent with expression results from metastatic patient samples (**Fig. 1D**). These same pathways, in addition to pathways that include complement and coagulation factors (which we see upregulated with *METTL3* knockdown; **Figs. 1D** and **4D**), make up a gastrointestinal-lineage transcriptional signature previously reported in prostate cancer by Shukala and colleagues This signature is regulated by HNF1A and HNF4G, and importantly leads to castration resistance (59). Upon closer examination of our RNA-seq data, we specifically see a significant upregulation in genes which are upregulated by both HNF1A and HNF4G in LNCaP cells (**Fig. 5E**; ref. 59). Although we do not see changes in the expression of either of these two transcription factors, we do see an upregulation of *NR5A2* (**Fig. 5F**), an important gastrointestinal transcription factor that has been shown to regulate the same pathways in breast and colon cancer cells (60, 61). Further, *NR5A2* (also known as *LRH-1*) has also been previously linked to CRPC, and in particular, overexpression of *NR5A2* in LNCaP cells rendered them resistant to the AR inhibitor bicalutamide, and to castration in a xenograft model (62). Examination of the patient data presented in **Fig. 1** also revealed that there is an inverse correlation with *NR5A2* and *METTL3* expression in samples of patients with CRPC (**Fig. 5G**).

Given these results, we then chose to examine how the *METTL3* knockdown lines respond at the cellular level to ENZ treatment, and if upregulation of *NR5A2* and these gene signatures leads to a resistant phenotype in our model. In the absence of *METTL3* knockdown, all three cell lines responded similarly to 10 μmol/L ENZ treatment, demonstrating an approximately 50% reduction in cell proliferation as compared with DMSO controls after 132 hours (**Fig. 5H**). Strikingly, upon doxycycline-induced expression of the *METTL3* shRNAs, both lines showed a significant (sh1, $P = 0.0012$; sh2, $P = 0.0011$) resistance to the ENZ treatment with only a 20% reduction in proliferation after 132 hours (**Fig. 5I**).

In order to determine the mechanism behind this phenotype, we combined our inducible knockdown of *METTL3* with transient knockdown via siRNAs. Given that our RNA-seq analysis demonstrated normal transcriptional responses of known AR-target genes in response to ENZ (**Fig. 5B**), we hypothesized that the mechanism of resistance to ENZ is independent of AR itself. This hypothesis was confirmed, in that combining knockdown of *AR* and *METTL3* did not significantly change the ability of the cells to proliferate in the presence of ENZ (Supplementary Fig. S5B). In contrast, knockdown of *NR5A2* resulted in a significant reduction in the ability of the *METTL3* knockdown lines to proliferate with ENZ treatment (**Fig. 5J**). Taken together, these findings suggest that knockdown of *METTL3* promotes ENZ resistance through an AR-independent upregulation of a gene signature driven by *NR5A2*.

Discussion

Current understanding of the effects of m^{6}A is that the mark mostly serves to destabilize mRNAs (16, 55). As such, we would expect to see

increases in the expression of methylated genes with *METTL3* knockdown. Strikingly, in our data, we see relatively few changes in mRNA expression with *METTL3* knockdown. Furthermore, although changes in the translation of methylated transcripts are generally rarer, they predominantly serve to increase TE. Again, we would then expect to see a decrease in TE, whereas we see many increases at the level of TE and protein with *METTL3* knockdown in prostate cancer. It therefore remains likely that we are also identifying some secondary-level changes due to alterations in the expression of upstream m⁶A methylated genes. It should also be noted that overall, our expression changes are fewer and more modest than many published studies. We propose that this is likely due to the fact that we are engineering an approximately 70% to 80% knockdown instead of a complete *METTL3* knockout. In support of these hypotheses, we attempted to determine whether *METTL3* knockdown altered the levels of m⁶A on several candidate genes that were differentially regulated (*MFAP3, BCHE, NIPA2, SPON2, TMEM168,* and *ZNF460*) by m⁶A-IP followed by qPCR. Although we confirmed m⁶A methylation at all the annotated sites we queried, and saw a trend toward decreased enrichment on several transcripts with *METTL3* knockdown, they did not reach statistical significance ($n = 4$ independent experiments; Supplementary Fig. S6). It remains likely that the levels of knockdown we achieved elicit small but significant changes that are potentially below the sensitivity of this assay, or in a limited subset of genes beyond our candidates, but are sufficient to result in the observed phenotypic changes in these cells. Although it may be possible to see stronger effects on gene expression with a *METTL3* knockout, this phenotype is not clinically relevant as there is no complete loss of *METTL3* seen in patients with prostate cancer.

When examining pathways which are regulated by m⁶A in prostate cancer, we consistently saw enrichment for extracellular matrix (ECM) proteins in both our cell line models (**Figs. 3F, 4D,** and **5D**) and in patients with CRPC (**Fig. 1D**) with low levels of *METTL3*. Changes in the ECM are associated with increased tumor growth, migration, and invasion, allowing for metastatic progression (63, 64), including in prostate cancer (65). Furthermore, changes in the ECM have been implicated in therapy resistance in breast, ovarian, and prostate cancer (66–69). As such, it remains possible that these changes also contribute to the ENZ resistance demonstrated by the *METTL3* knockdown cells, and this would be a focus of future studies, in particular in a three-dimensional cell culture environment.

Last, our analysis of data related to patients with CRPC demonstrated an inverse correlation between the levels of *METTL3* and AR signaling. When we examined the interplay between m⁶A and AR signaling, we showed that though AR target genes and AR itself have relatively high numbers of annotated m⁶A sites, knockdown of *METTL3* did not change expression of these genes at the transcript or protein level. This may be due to low stoichiometry of the m⁶A sites on these transcripts (unresolved by miCLIP technology), redundancy with other components of the methyltransferase complex, or a lack of functionality of m⁶A on these transcripts. Nonetheless, we did find that knockdown of *METTL3* led to an upregulation of a previously identified gastrointestinal-lineage signature and rendered the cells resistant to ENZ in an AR-independent manner. Previously, this signature was shown to be driven by HNF4G and HNF1A which were induced in response to androgen deprivation (59). Here, we hypothesize that this signature is driven by an upregulation of another GI-lineage transcription factor *NR5A2* in response to *METTL3* knockdown. Although

NR5A2 itself was not identified as a methylated transcript in our miCLIP analysis, it is worth noting that the basal expression of *NR5A2* in LNCaP cells is relatively low. Therefore, it is possible that any potential methylation of this transcript may evade detection with an IP-based approach. Nonetheless, it also plausible that *METTL3* knockdown is altering the methylation a yet unidentified upstream regulator of *NR5A2* as opposed to the gene itself. The exact mechanism behind how this signature leads to ENZ resistance remains to be determined. However, among the included genes are those involved in both the metabolism of steroid hormones (i.e., *AKR1C3* and *UGT2B15*) and general drug metabolism (i.e., *GSTA1, GSTA2, GSTK1*) both of which would play a probable role in ENZ resistance.

In summary, in this study we identified many genes and pathways which are dysregulated in the context of low *METTL3* expression in prostate cancer. In particular, we have nominated extracellular matrix proteins as being highly influenced by changes in *METTL3* expression. Furthermore, we showed that combining *METTL3* knockdown and ENZ treatment led to an AR-independent upregulation of a GI-specific gene signature driven by *NR5A2* and rendered the cells resistant to ENZ. Future work will focus on delineating the precise mechanism behind the ENZ-resistant phenotype in an attempt to determine whether *NR5A2* and/or other downstream pathway genes may function as potential therapeutic targets in CRPC. Overall, these findings support a new role for m⁶A in regulating therapeutic sensitivity to ARSi and furthermore suggest that patients with low levels of *METTL3* expression may differentially respond to ARSi.

Authors' Contributions

K.A. Cotter: Conceptualization, formal analysis, investigation, writing–original draft. **J. Gallon:** Formal analysis. **N. Uebersax:** Investigation. **P. Rubin:** Investigation. **K.D. Meyer:** Formal analysis. **S. Piscuoglio:** Formal analysis. **S.R. Jaffrey:** Conceptualization, writing–review and editing. **M.A. Rubin:** Conceptualization, writing–original draft, writing–review and editing.

References

1. Baca SC, Prandi D, Lawrence MS, Mosquera JM, Romanel A, Drier Y, et al. Punctuated evolution of prostate cancer genomes. Cell 2013;153:666–77.

2. Berger MF, Lawrence MS, Demichelis F, Drier Y, Cibulskis K, Sivachenko AY, et al. The genomic complexity of primary human prostate cancer. Nature 2011; 470:214–20.

3. Barbieri CE, Baca SC, Lawrence MS, Demichelis F, Blattner M, Theurillat J-P, et al. Exome sequencing identifies recurrent SPOP, FOXA1 and MED12 mutations in prostate cancer. Nat Genet 2012;44:685–9.

4. Chalmers ZR, Connelly CF, Fabrizio D, Gay L, Ali SM, Ennis R, et al. Analysis of 100,000 human cancer genomes reveals the landscape of tumor mutational burden. Genome Med 2017;9:34.

5. Varambally S, Yu J, Laxman B, Rhodes DR, Mehra R, Tomlins SA, et al. Integrative genomic and proteomic analysis of prostate cancer reveals signatures of metastatic progression. Cancer Cell 2005;8:393–406.

6. Sinha A, Huang V, Livingstone J, Wang J, Fox NS, Kurganovs N, et al. The proteogenomic landscape of curable prostate cancer. Cancer Cell 2019;35:414–427 e416.

7. Desrosiers R, Friderici K, Rottman F. Identification of methylated nucleosides in messenger RNA from Novikoff hepatoma cells. Proc Natl Acad Sci U S A 1974; 71:3971–5.

8. Bokar JA, Shambaugh ME, Polayes D, Matera AG, Rottman FM. Purification and cDNA cloning of the AdoMet-binding subunit of the human mRNA (N6-adenosine)-methyltransferase. RNA 1997;3:1233–47.

9. Liu J, Yue Y, Han D, Wang X, Fu Y, Zhang L, et al. A METTL3-METTL14 complex mediates mammalian nuclear RNA N6-adenosine methylation. Nat Chem Biol 2014;10:93–5.

10. Ping X-L, Sun B-F, Wang L, Xiao W, Yang X, Wang W-J, et al. Mammalian WTAP is a regulatory subunit of the RNA N6-methyladenosine methyltransferase. Cell Res 2014;24:177–89.

11. Schwartz S, Mumbach MR, Jovanovic M, Wang T, Maciag K, Bushkin GG, et al. Perturbation of m6A writers reveals two distinct classes of mRNA methylation at internal and 5' sites. Cell Rep 2014;8:284–96.

12. Wang Y, Li Y, Toth JI, Petroski MD, Zhang Z, Zhao JC. N6-methyladenosine modification destabilizes developmental regulators in embryonic stem cells. Nat Cell Biol 2014;16:191–8.

13. Zheng G, Dahl JA, Niu Y, Fedorcsak P, Huang C-M, Li CJ, et al. ALKBH5 is a mammalian RNA demethylase that impacts RNA metabolism and mouse fertility. Mol Cell 2013;49:18–29.

14. Dominissini D, Moshitch-Moshkovitz S, Schwartz S, Salmon-Divon M, Ungar L, Osenberg S, et al. Topology of the human and mouse m6A RNA methylomes revealed by m6A-seq. Nature 2012;485:201–6.

15. Wang X, Lu Z, Gomez A, Hon GC, Yue Y, Han D, et al. N6-methyladenosine-dependent regulation of messenger RNA stability. Nature 2014;505:117–20.

16. Zaccara S, Jaffrey SR. A unified model for the function of YTHDF proteins in regulating m(6)A-modified mRNA. Cell 2020;181:1582–95.e18.

17. Wang X, Zhao BS, Roundtree IA, Lu Z, Han D, Ma H, et al. N(6)-methyladenosine modulates messenger RNA translation efficiency. Cell 2015;161:1388–99.

18. Zhao X, Yang Y, Sun B-F, Shi Y, Yang X, Xiao W, et al. FTO-dependent demethylation of N6-methyladenosine regulates mRNA splicing and is required for adipogenesis. Cell Res 2014;24:1403–19.

19. Alarcon CR, Lee H, Goodarzi H, Halberg N, Tavazoie SF. N6-methyladenosine marks primary microRNAs for processing. Nature 2015;519:482–5.

20. Cui Q, Shi H, Ye P, Li L, Qu Q, Sun G, et al. m6A RNA methylation regulates the self-renewal and tumorigenesis of glioblastoma stem cells. Cell Rep 2017;18: 2622–34.

21. Zhang C, Samanta D, Lu H, Bullen JW, Zhang H, Chen I, et al. Hypoxia induces the breast cancer stem cell phenotype by HIF-dependent and ALKBH5-mediated m(6)A-demethylation of NANOG mRNA. Proc Natl Acad Sci U S A 2016;113:E2047–56.

22. Zhang S, Zhao BS, Zhou A, Lin K, Zheng S, Lu Z, et al. m6A demethylase ALKBH5 maintains tumorigenicity of glioblastoma stem-like cells by sustaining FOXM1 expression and cell proliferation program. Cancer Cell 2017;31:591–606.e596.

23. Lin S, Choe J, Du P, Triboulet R, Gregory RI. The m(6)A methyltransferase METTL3 promotes translation in human cancer cells. Mol Cell 2016;62:335–45.

24. Vu LP, Pickering BF, Cheng Y, Zaccara S, Nguyen D, Minuesa G, et al. The N(6)-methyladenosine (m(6)A)-forming enzyme METTL3 controls myeloid differentiation of normal hematopoietic and leukemia cells. Nat Med 2017; 23:1369–76.

25. Barbieri I, Tzelepis K, Pandolfini L, Shi J, Millán-Zambrano G, Robson SC, et al. Promoter-bound METTL3 maintains myeloid leukaemia by m(6)A-dependent translation control. Nature 2017;552:126–31.

26. Cai J, Yang F, Zhan H, Situ J, Li W, Mao Y, et al. RNA m(6)A methyltransferase METTL3 promotes the growth of prostate cancer by regulating hedgehog pathway. Onco Targets Ther 2019;12:9143–52.

27. Yuan Y, Du Y, Wang L, Liu X. The M6A methyltransferase METTL3 promotes the development and progression of prostate carcinoma via mediating MYC methylation. J Cancer 2020;11:3588–95.

28. Scher HI, Sawyers CL. Biology of progressive, castration-resistant prostate cancer: directed therapies targeting the androgen-receptor signaling axis. J Clin Oncol 2005;23:8253–61.

29. Rubin MA, Bristow RG, Thienger PD, Dive C, Imielinski M. Impact of lineage plasticity to and from a neuroendocrine phenotype on progression and response in prostate and lung cancers. Mol Cell 2020;80:P562–77.

30. Roviello G, Sigala S, Sandhu S, Bonetta A, Cappelletti MR, Zanotti L, et al. Role of the novel generation of androgen receptor pathway targeted agents in the management of castration-resistant prostate cancer: A literature based meta-analysis of randomized trials. Eur J Cancer 2016;61:111–21.

31. Linder B, Grozhik AV, Olarerin-George AO, Meydan C, Mason CE, Jaffrey SR. Single-nucleotide-resolution mapping of m6A and m6Am throughout the transcriptome. Nat Methods 2015;12:767–72.

32. Olarerin-George AO, Jaffrey SRMetaPlotR: a Perl/R pipeline for plotting meta-genes of nucleotide modifications and other transcriptomic sites. Bioinformatics 2017;33:1563–4.

33. Dobin A, Davis CA, Schlesinger F, Drenkow J, Zaleski C, Jha S, et al. STAR: ultrafast universal RNA-seq aligner. Bioinformatics 2013;29:15–21.

34. Li B, Dewey CNRSEM: accurate transcript quantification from RNA-seq data with or without a reference genome. BMC Bioinformatics 2011;12:323.

35. Love MI, Huber W, Anders S. Moderated estimation of fold change and dispersion for RNA-seq data with DESeq2. Genome Biol 2014;15:550.

36. Li W, Wang W, Uren PJ, Penalva LOF, Smith ADRiborex: fast and flexible identification of differential translation from Ribo-seq data. Bioinformatics 2017; 33:1735–7.

37. Cox J, Mann MMaxQuant enables high peptide identification rates, individualized p.p.b.-range mass accuracies and proteome-wide protein quantification. Nat Biotechnol 2008;26:1367–72.

38. UniProt CUniProt: a worldwide hub of protein knowledge. Nucleic Acids Res 2019;47:D506–15.

39. Silva JC, Gorenstein MV, Li GZ, Vissers JP, Geromanos SJ. Absolute quantification of proteins by LCMSE: a virtue of parallel MS acquisition. Mol Cell Proteomics 2006;5:144–56.

40. Huber W, von Heydebreck A, Sultmann H, Poustka A, Vingron M. Variance stabilization applied to microarray data calibration and to the quantification of differential expression. Bioinformatics 2002;18 Suppl 1:S96–104.

41. Kammers K, Cole RN, Tiengwe C, Ruczinski I. Detecting significant changes in protein abundance. EuPA Open Proteom 2015;7:11–19.

42. Benjamini Y, Hochberg Y. Controlling the false discovery rate: a practical and powerful approach to multiple testing. J R Stat Soc Series B Stat Methodol 1995; 57:289–300.

43. Abida W, Cyrta J, Heller G, Prandi D, Armenia J, Coleman I, et al. Genomic correlates of clinical outcome in advanced prostate cancer. Proc Natl Acad Sci U S A 2019;116:11428–36.

44. Beltran H, Prandi D, Mosquera JM, Benelli M, Puca L, Cyrta J, et al. Divergent clonal evolution of castration-resistant neuroendocrine prostate cancer. Nat Med 2016;22:298–305.

45. Meyer KD, Saletore Y, Zumbo P, Elemento O, Mason CE, Jaffrey SR. Comprehensive analysis of mRNA methylation reveals enrichment in 3' UTRs and near stop codons. Cell 2012;149:1635–46.

46. Ingolia NT, Ghaemmaghami S, Newman JR, Weissman JS. Genome-wide analysis in vivo of translation with nucleotide resolution using ribosome profiling. Science 2009;324:218–23.

47. Rooijers K, Loayza-Puch F, Nijtmans LG, Agami R. Ribosome profiling reveals features of normal and disease-associated mitochondrial translation. Nat Commun 2013;4:2886.

48. McDermott JE, Arshad OA, Petyuk VA, Fu Y, Gritsenko MA, Clauss TR, et al. Proteogenomic characterization of ovarian HGSC implicates mitotic kinases, replication stress in observed chromosomal instability. Cell Rep Med 2020;1: 100004.

49. Mertins P, Mani DR, Ruggles KV, Gillette MA, Clauser KR, Wang P, et al. Proteogenomics connects somatic mutations to signalling in breast cancer. Nature 2016;534:55–62.

50. Zhang B, Wang J, Wang X, Zhu J, Liu Q, Shi Z, et al. Proteogenomic characterization of human colon and rectal cancer. Nature 2014;513:382–7.

51. Rubio RM, Depledge DP, Bianco C, Thompson L, Mohr I. RNA m(6) A modification enzymes shape innate responses to DNA by regulating interferon beta. Genes Dev 2018;32:1472–84.

52. Winkler R, Gillis E, Lasman L, Safra M, Geula S, Soyris C, et al. m(6)A modification controls the innate immune response to infection by targeting type I interferons. Nat Immunol 2019;20:173–82.

53. Danziger O, Shai B, Sabo Y, Bacharach E, Ehrlich M. Combined genetic and epigenetic interferences with interferon signaling expose prostate cancer cells to viral infection. Oncotarget 2016;7:52115–34.

54. Dunn GP, Sheehan KC, Old LJ, Schreiber RD. IFN unresponsiveness in LNCaP cells due to the lack of JAK1 gene expression. Cancer Res 2005;65:3447–53.

55. Lasman L, Krupalnik V, Viukov S, Mor N, Aguilera-Castrejon A, Schneir D, et al. Context-dependent functional compensation between Ythdf m(6)A reader proteins. Genes Dev 2020;34:1373–91.

56. Shen MM, Abate-Shen C. Roles of the Nkx3.1 homeobox gene in prostate organogenesis and carcinogenesis. Dev Dyn 2003;228:767–78.

57. Kregel S, Chen JL, Tom W, Krishnan V, Kach J, Brechka H, et al. Acquired resistance to the second-generation androgen receptor antagonist enzalutamide in castration-resistant prostate cancer. Oncotarget 2016;7:26259–74.

58. Kohrt SE, Awadallah WN, Phillips RA, Case TC, Jin R, Nanda JS, et al. Identification of genes required for enzalutamide resistance in castration-resistant prostate cancer cells in vitro. Mol Cancer Ther 2020;20:398–409.

59. Shukla S, Cyrta J, Murphy DA, Walczak EG, Ran L, Agrawal P, et al. Aberrant activation of a gastrointestinal transcriptional circuit in prostate cancer mediates castration resistance. Cancer Cell 2017;32:792–806.e797.

60. Bayrer JR, Mukkamala S, Sablin EP, Webb P, Fletterick RJ. Silencing LRH-1 in colon cancer cell lines impairs proliferation and alters gene expression programs. Proc Natl Acad Sci U S A 2015;112:2467–72.

61. Bianco S, Brunelle M, Jangal M, Magnani L, Gevry N. LRH-1 governs vital transcriptional programs in endocrine-sensitive and -resistant breast cancer cells. Cancer Res 2014;74:2015–25.

62. Xiao L, Wang Y, Xu K, Hu H, Xu Z, Wu D, et al. Nuclear Receptor LRH-1 functions to promote castration-resistant growth of prostate cancer via its promotion of intratumoral androgen biosynthesis. Cancer Res 2018;78: 2205–18.

63. Kai F, Drain AP, Weaver VM. The extracellular matrix modulates the metastatic journey. Dev Cell 2019;49:332–46.

64. Winkler J, Abisoye-Ogunniyan A, Metcalf KJ, Werb Z. Concepts of extracellular matrix remodelling in tumour progression and metastasis. Nat Commun 2020; 11:5120.

65. Penet MF, Kakkad S, Pathak AP, Krishnamachary B, Mironchik Y, Raman V, et al. Structure and function of a prostate cancer dissemination-permissive extracellular matrix. Clin Cancer Res 2017;23:2245–54.

66. Hanker AB, Estrada MV, Bianchini G, Moore PD, Zhao J, Cheng F, et al. Extracellular matrix/integrin signaling promotes resistance to combined inhibition of HER2 and PI3K in HER2(+) breast cancer. Cancer Res 2017; 77:3280–92.

67. Januchowski R, Zawierucha P, Rucinski M, Nowicki M, Zabel M. Extracellular matrix proteins expression profiling in chemoresistant variants of the A2780 ovarian cancer cell line. Biomed Res Int 2014;2014:365867.

68. Joyce MH, Lu C, James ER, Hegab R, Allen SC, Suggs LJ, et al. Phenotypic basis for matrix stiffness-dependent chemoresistance of breast cancer cells to doxorubicin. Front Oncol 2018;8:337.

69. Mosquera MJ, Bareja R, Bernheim J, Asad M, Cheung C, Sigouros M, et al. Extracellular microenvironment in patient-derived hydrogel organoids of prostate cancer regulates therapeutic response. medRxiv 2020.

70. Edgar R, Domrachev M, Lash AE. Gene expression omnibus: NCBI gene expression and hybridization array data repository. Nucleic Acids Res 2002; 30:207–10.

71. Perez-Riverol Y, Csordas A, Bai J, Bernal-Llinares M, Hewapathirana S, Kundu DJ, et al. The PRIDE database and related tools and resources in 2019: improving support for quantification data. Nucleic Acids Res 2019;47: D442–50.

72. Hieronymus H, Lamb J, Ross KN, Peng XP, Clement C, Rodina A, et al. Gene expression signature-based chemical genomic prediction identifies a novel class of HSP90 pathway modulators. Cancer Cell 2006;10:321–30.